

Supplementary Material

Predictions of the chiral self-assembling of TPPS₄ porphyrin aggregates perturbed by molecular rotations

Gioacchino Schifino¹, Mariagrazia Fortino¹, Luigi Monsù Scolaro², Adriana Pietropaolo^{1*}

AFFILIATIONS

¹ Dipartimento di Scienze della salute, Università Magna Græcia di Catanzaro, Viale Europa, Catanzaro.

² Dipartimento di Scienze Chimiche, biologiche, farmaceutiche e ambientali Università degli Studi di Messina, V.le F. Stagno D'Alcontres 31, Vill. S. Agata, Messina

***Authors to whom correspondence should be addressed:**

apietropaolo@unicz.it,

Contents

1. Figure of the potential energy scan describing the rotations of the sulfonatophenyl substituents attached to the porphyrin macrocycle	1
2. Figure of the chosen collective variables	1
3. Figures of the evolution of the dihedral angles	2
4. Figures of the evolution of the distances between two porphyrins	5
5. Figures of the evolution of the tilting angles	9
6. Figures of the free-energy profiles	12

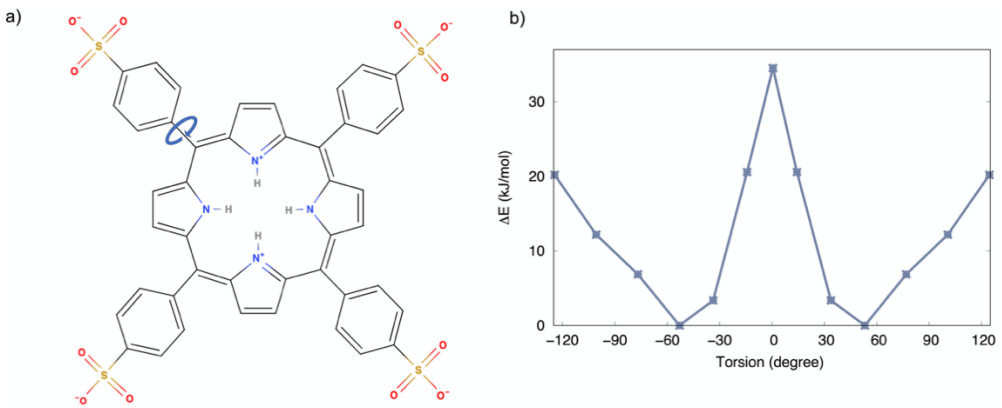


Figure S1. a) A sketch of the $\text{H}_4\text{TPPS}_4^{2-}$ molecule under study. b) Adiabatic free-energy barriers related to the internal rotation of a single meso-sulfonatophenyl group attached to a porphyrin macrocycle.

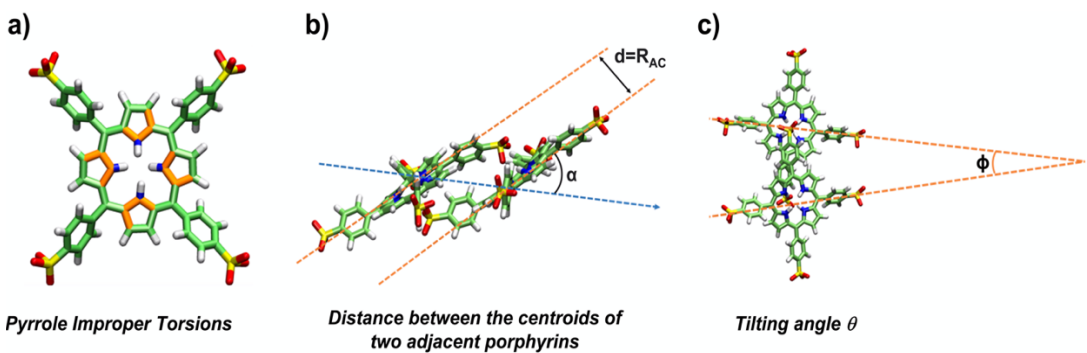


Figure S2. a) The four pyrrole torsions identifying the collective variables for the free-energy simulations. b)-c) The stacking distance and tilting angle defining the J-aggregate.

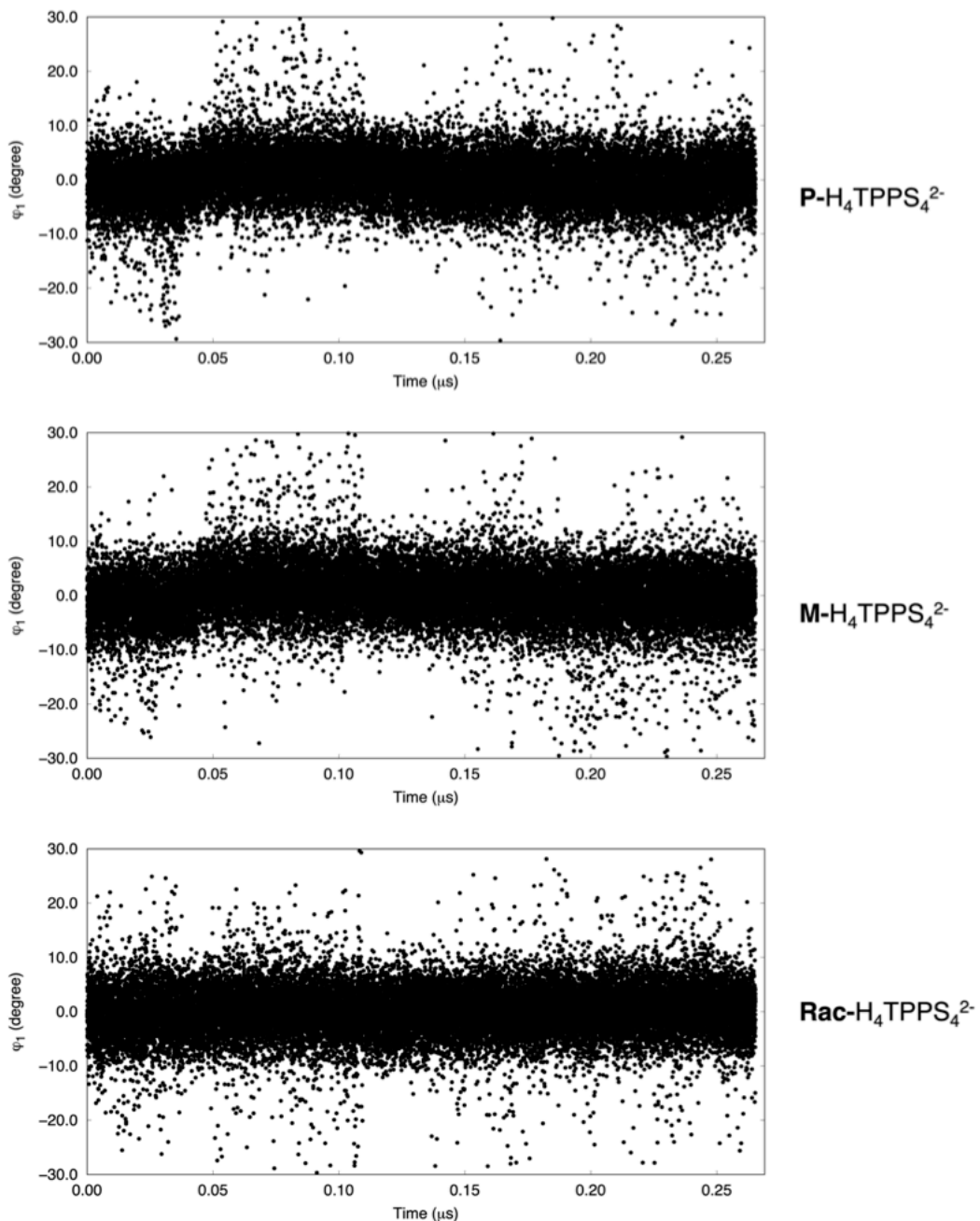


Figure S3. Variation of the representative dihedrals (pyrrole dihedral angles ϕ_1) of a **P-** $\text{H}_4\text{TPPS}_4^{2-}$ (replica 1) **M-** $\text{H}_4\text{TPPS}_4^{2-}$ (replica 2) and **Rac-** $\text{H}_4\text{TPPS}_4^{2-}$ (replica 3) monomers as a function of the simulation progress, for the free-energy simulations.

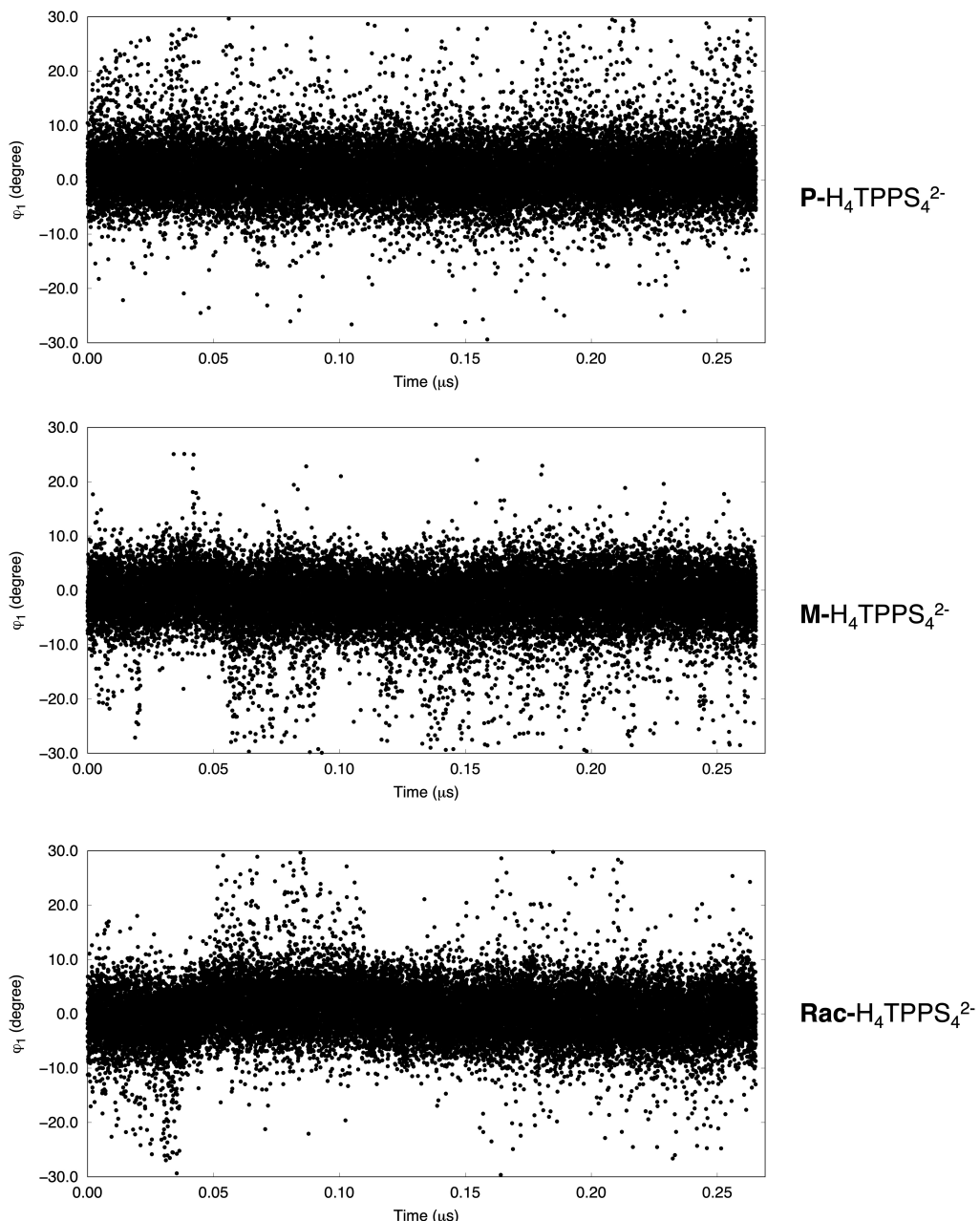


Figure S4. Variation of the representative dihedrals (pyrrole dihedral angles ϕ_1) of a **P-** $\text{H}_4\text{TPPS}_4^{2-}$ **M-** $\text{H}_4\text{TPPS}_4^{2-}$ and **Rac-** $\text{H}_4\text{TPPS}_4^{2-}$ dimers as a function of the simulation progress, for the free-energy simulations.

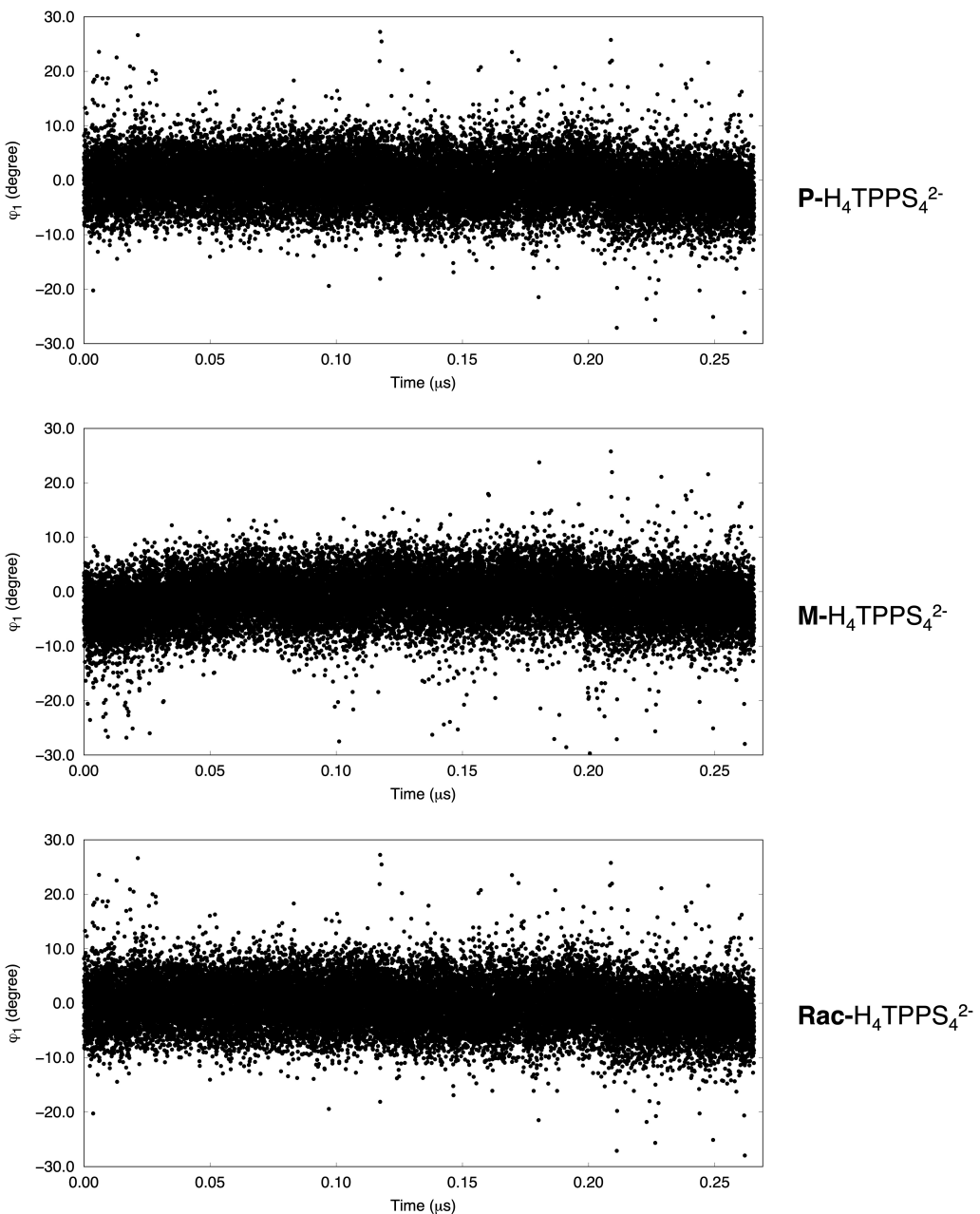


Figure S5. Variation of the representative dihedrals (pyrrole dihedral angles ϕ_1) of a **P-** H₄TPPS₄²⁻ **M-** H₄TPPS₄²⁻ and **Rac-** H₄TPPS₄²⁻ trimers as a function of the simulation progress, for the free-energy simulations.

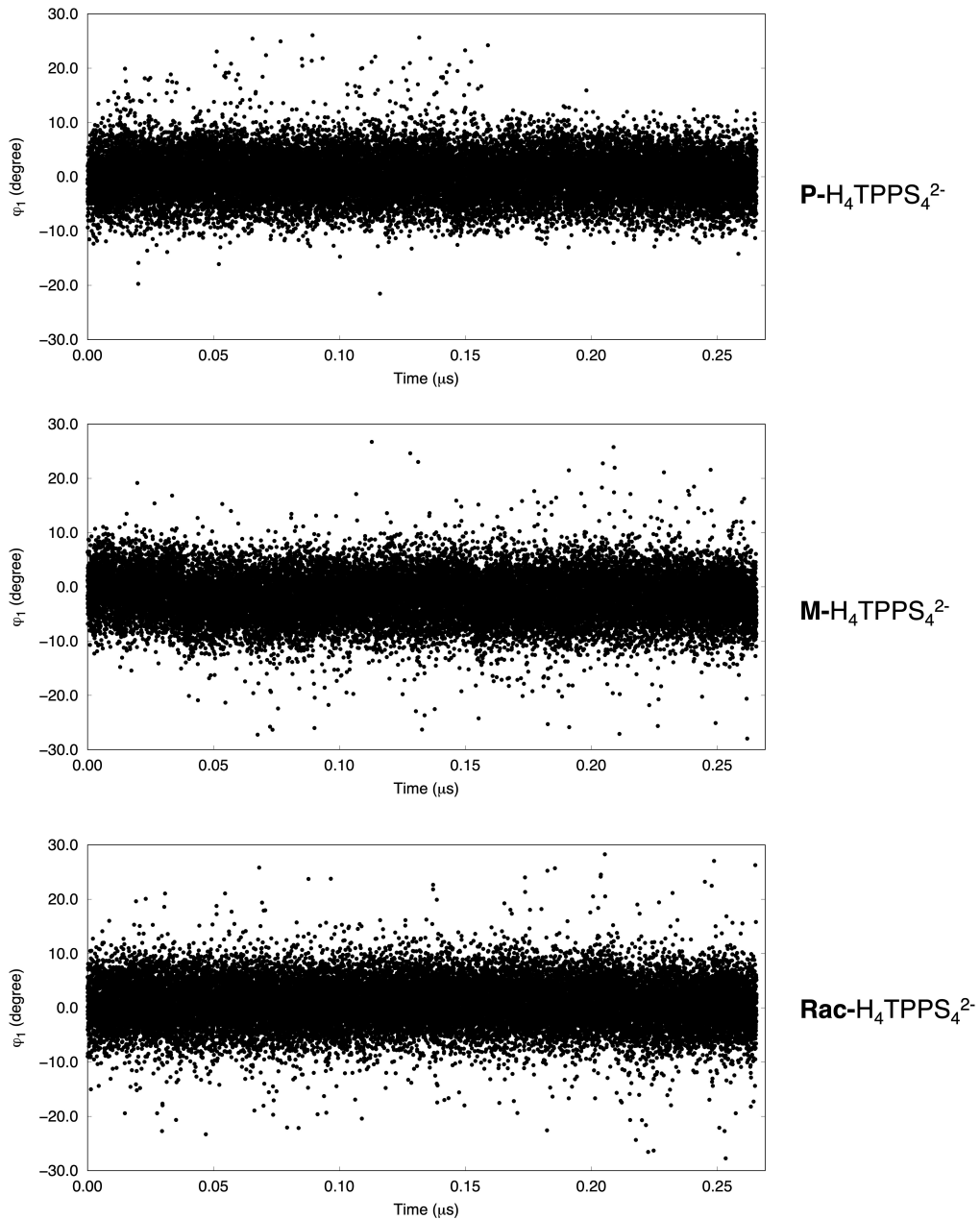


Figure S6. Variation of the representative dihedrals (pyrrole dihedral angles ϕ_1) of a **P-** H₄TPPS₄²⁻ **M-** H₄TPPS₄²⁻ and **Rac-** H₄TPPS₄²⁻ tetramers as a function of the simulation progress, for the free-energy simulations.

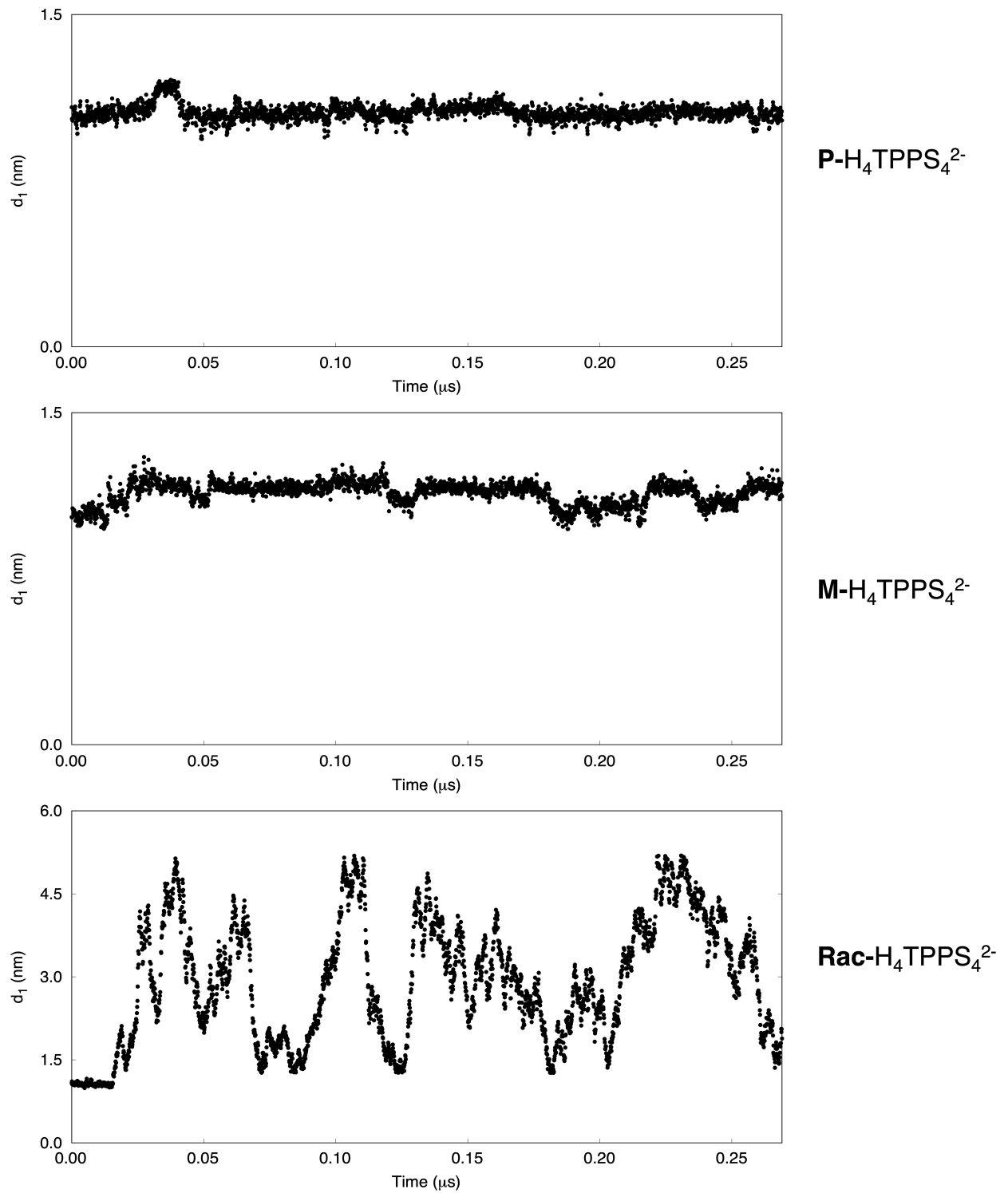


Figure S7. Variation of the representative distance between two adjacent porphyrins of a **P**- $\text{H}_4\text{TPPS}_4^{2-}$, **M**- $\text{H}_4\text{TPPS}_4^{2-}$ and **Rac**- $\text{H}_4\text{TPPS}_4^{2-}$ dimers as a function of the simulation progress, for the free-energy simulations.

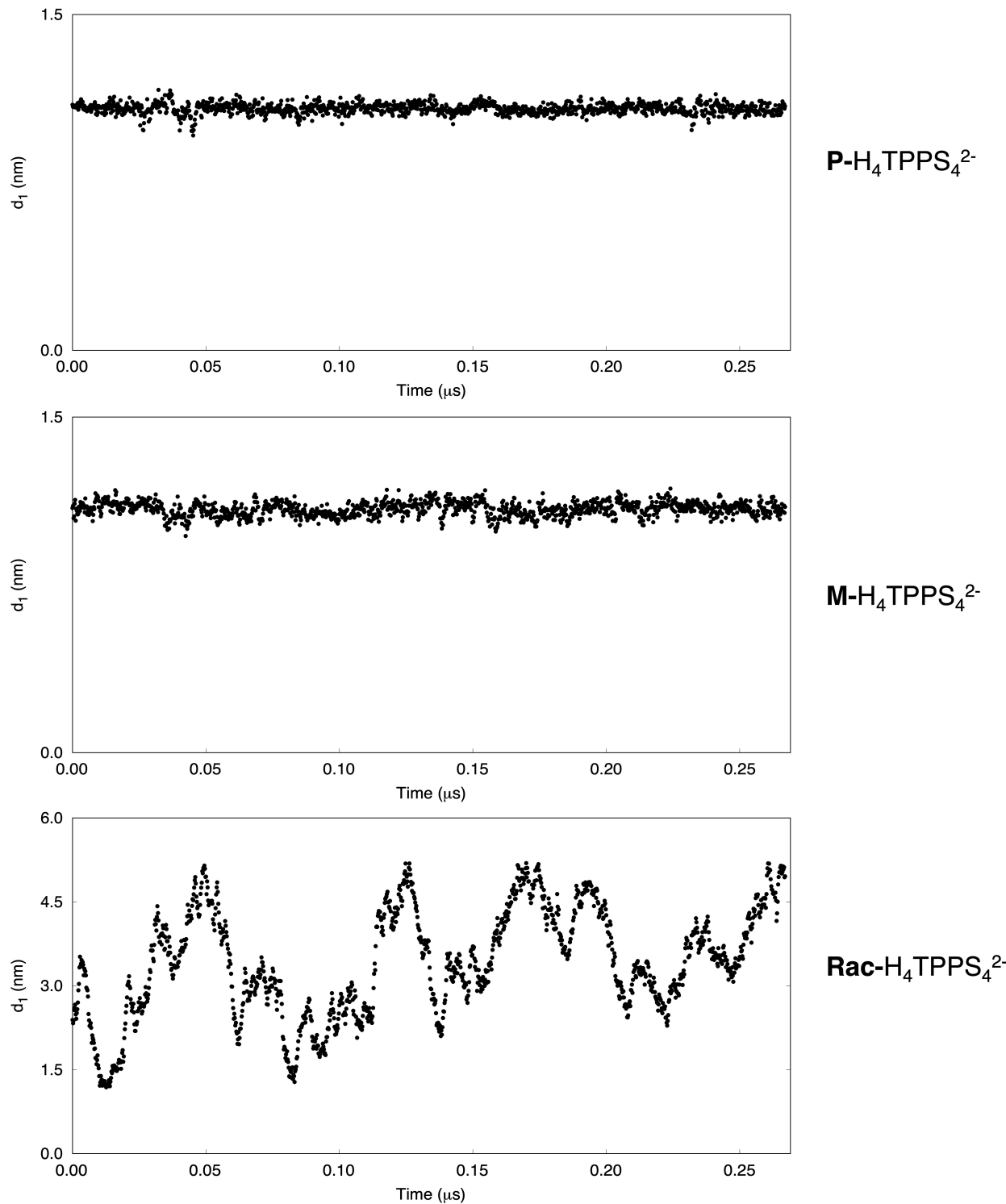


Figure S8. Variation of the representative distance between two adjacent porphyrins of a **P**- $\text{H}_4\text{TPPS}_4^{2-}$, **M**- $\text{H}_4\text{TPPS}_4^{2-}$ and **Rac**- $\text{H}_4\text{TPPS}_4^{2-}$ trimers as a function of the simulation progress, for the free-energy simulations.

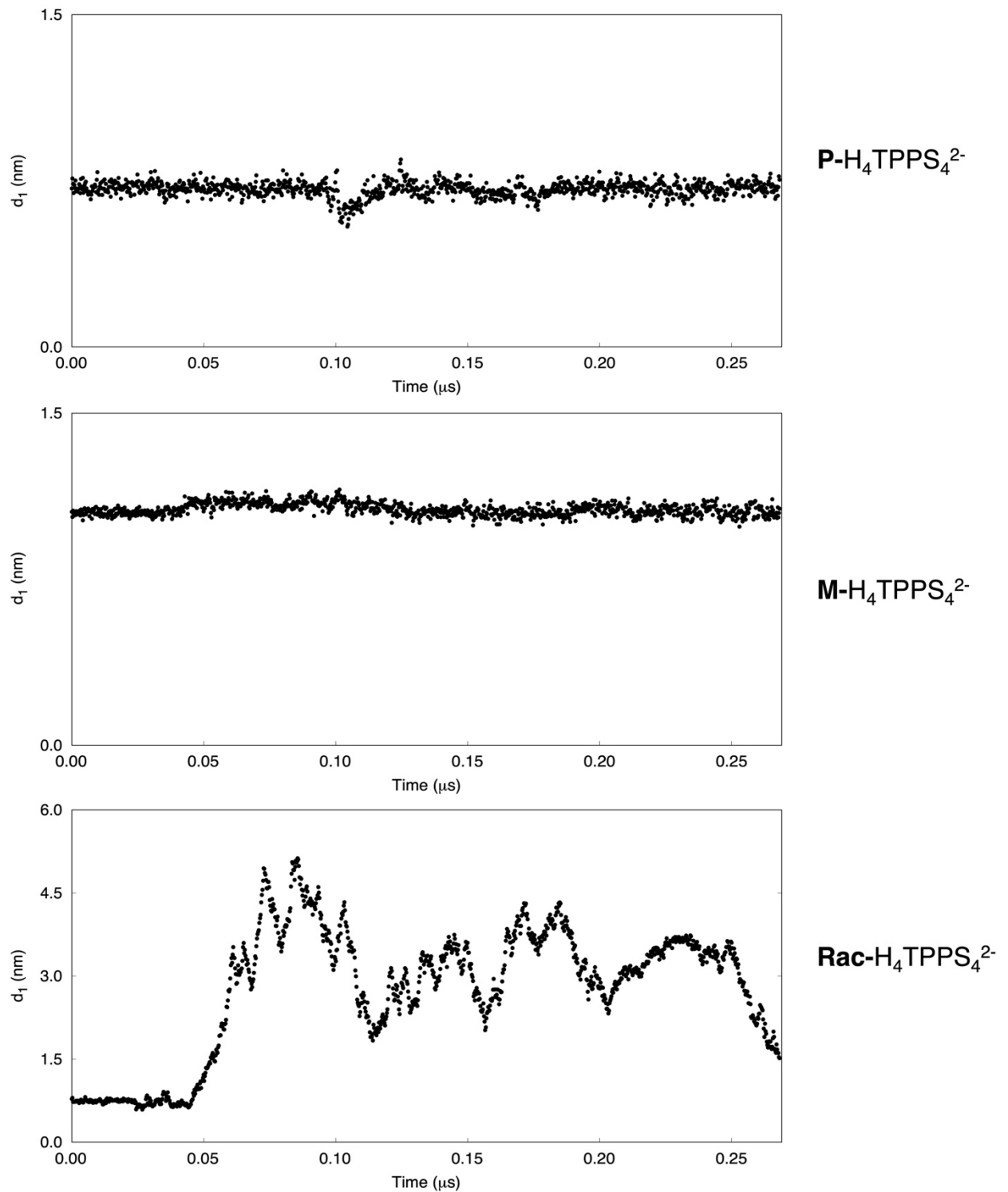


Figure S9. Variation of the representative distance between two adjacent porphyrins of a **P**- $\text{H}_4\text{TPPS}_4^{2-}$ **M**- $\text{H}_4\text{TPPS}_4^{2-}$ and **Rac**- $\text{H}_4\text{TPPS}_4^{2-}$ tetramers as a function of the simulation progress, for the free-energy simulations.

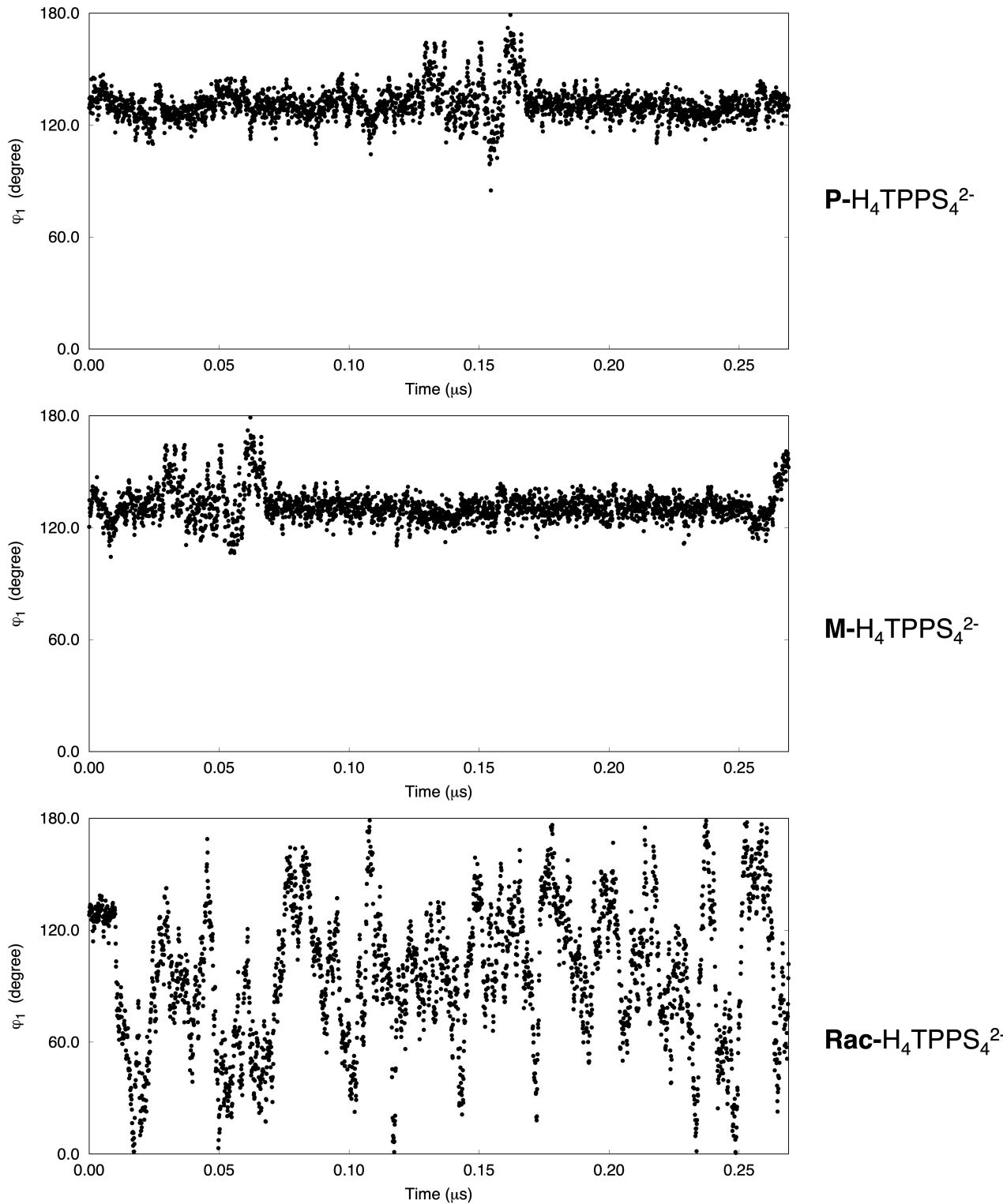


Figure S10. Variation of the representative tilting angle of a **P**- $\text{H}_4\text{TPPS}_4^{2-}$ **M**- $\text{H}_4\text{TPPS}_4^{2-}$ and **Rac**- $\text{H}_4\text{TPPS}_4^{2-}$ dimers as a function of the simulation progress, for the free-energy simulations.

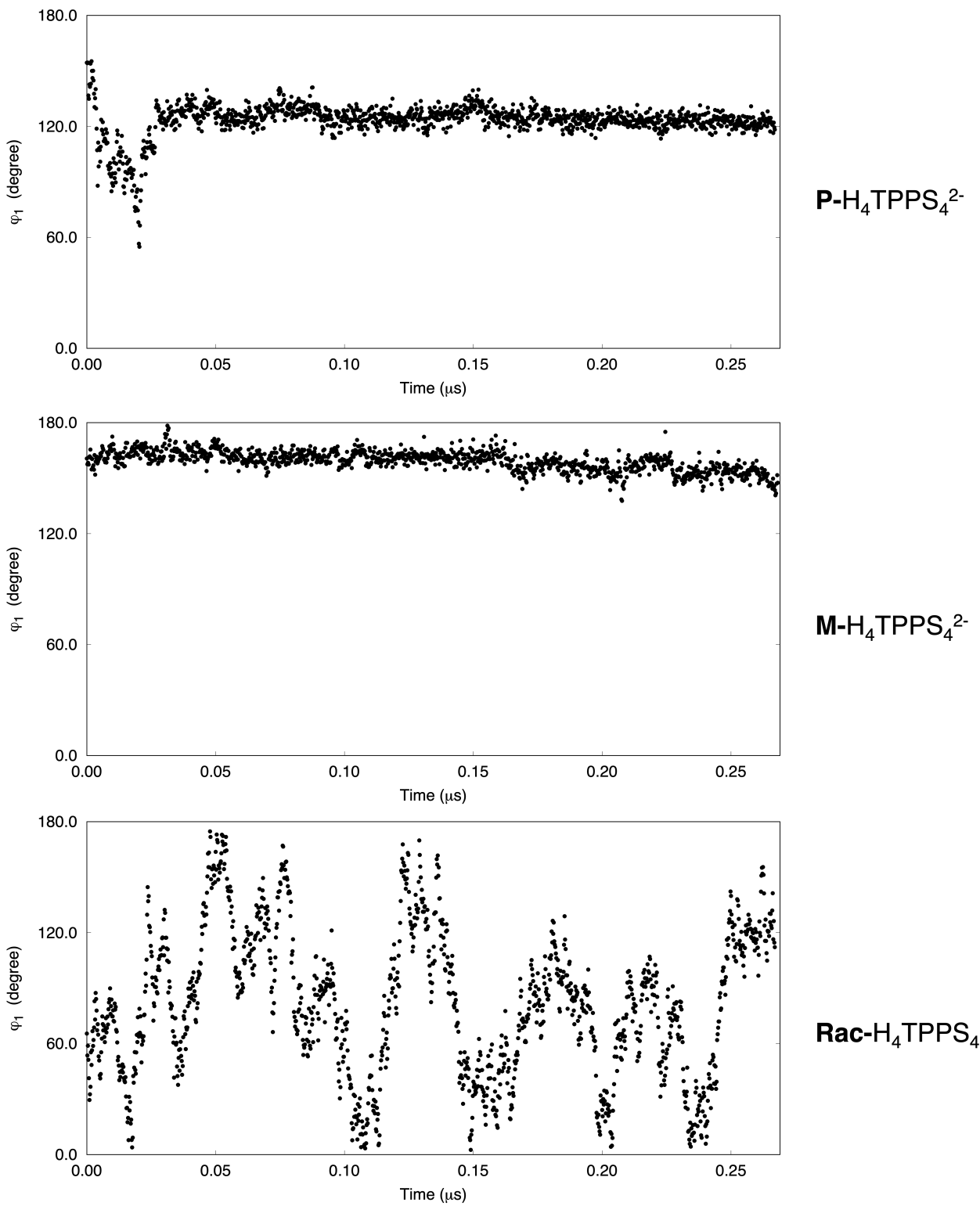


Figure S11. Variation of the representative tilting angle of a **P-** H₄TPPS₄²⁻ **M-** H₄TPPS₄²⁻ and **Rac-** H₄TPPS₄²⁻ trimers as a function of the simulation progress, for the free-energy simulations.

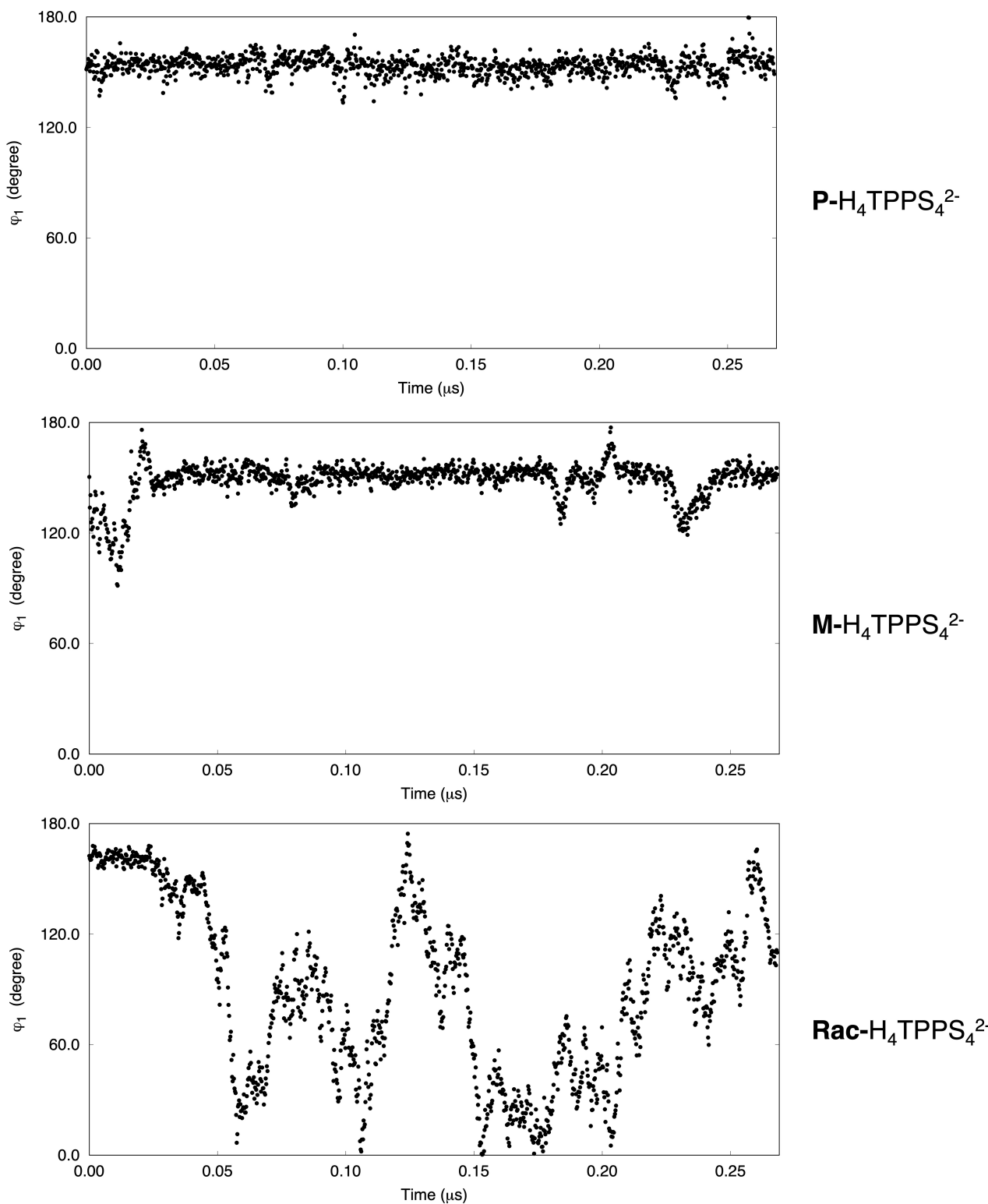


Figure S12. Variation of the representative tilting angle of a **P-** $\text{H}_4\text{TPPS}_4^{2-}$ **M-** $\text{H}_4\text{TPPS}_4^{2-}$ and **Rac-** $\text{H}_4\text{TPPS}_4^{2-}$ tetramers as a function of the simulation progress, for the free-energy simulations.

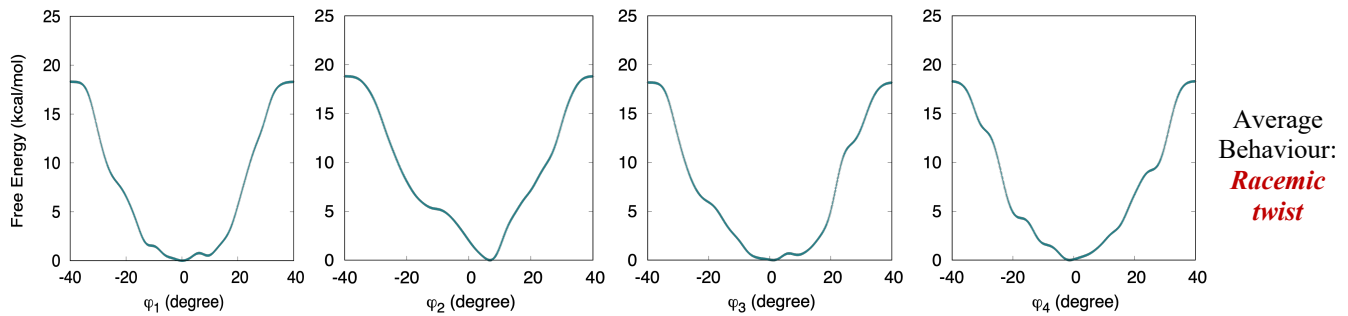


Figure S13. Mono-dimensional free-energy profiles computed for the **P-H₄TPPS₄²⁻** monomer using the PB-MetaD approach, as a function of the pyrrole dihedral angles $\phi_1, \phi_2, \phi_3, \phi_4$. These maps have been constructed considering the data of **P-H₄TPPS₄²⁻**, with all the four sulfonato-phenyl dihedral angles positive.

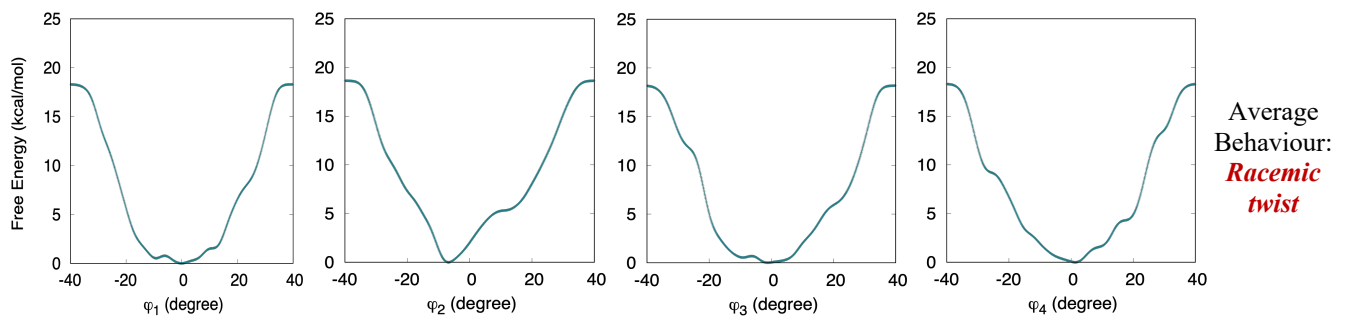


Figure S14. Mono-dimensional free-energy profiles computed for the **M-H₄TPPS₄²⁻** monomer using the PB-MetaD approach, as a function of the pyrrole dihedral angles $\phi_1, \phi_2, \phi_3, \phi_4$. These maps have been constructed considering the data of **M-H₄TPPS₄²⁻**, with all the four sulfonato-phenyl dihedral angles negative.

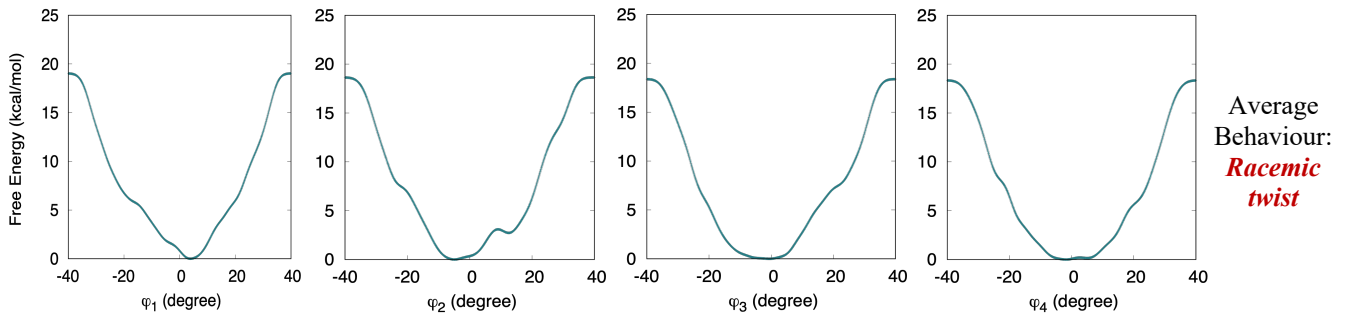


Figure S15. Mono-dimensional free-energy profiles computed for the **Rac-H₄TPPS₄²⁻** monomer using the PB-MetaD approach, as a function of the pyrrole dihedral angles $\phi_1, \phi_2, \phi_3, \phi_4$. These maps have been constructed considering the data of **Rac-H₄TPPS₄²⁻**, with two sulfonato-phenyl dihedral angles positive and two negative.

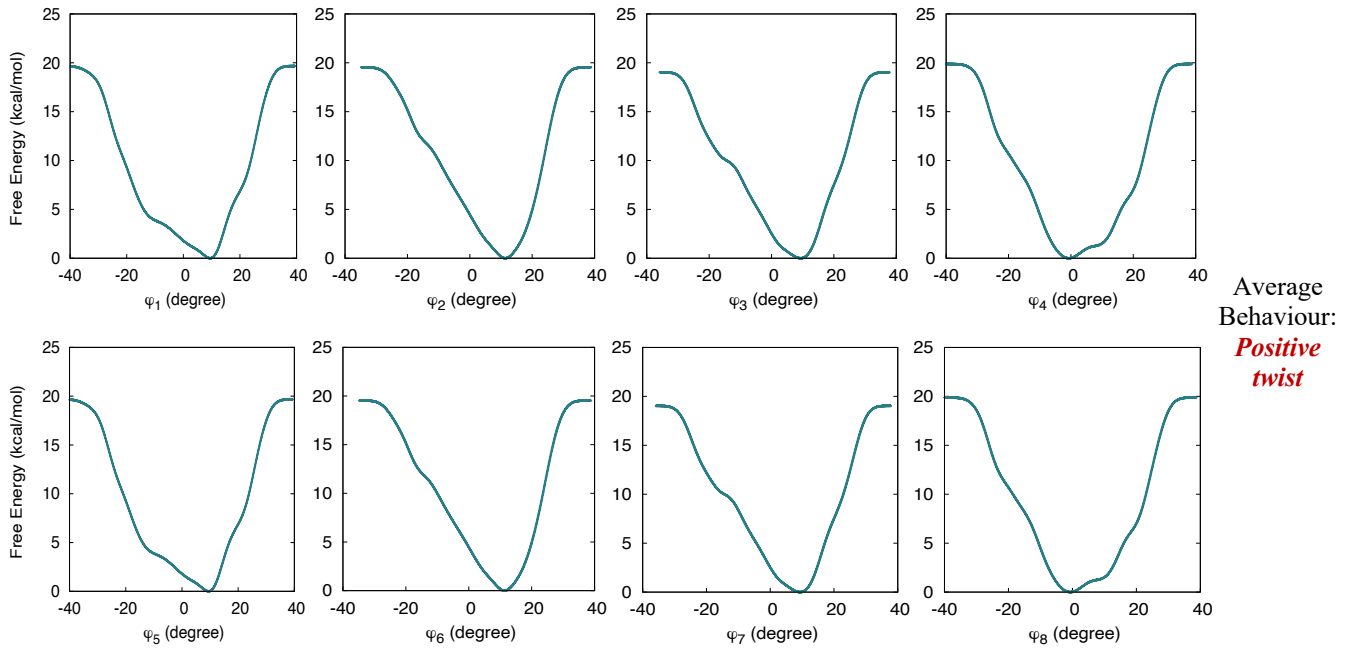


Figure S16. Monodimensional Free-energy profiles computed for the **P-H₄TPPS₄²⁻** dimer within the PB-MetaD approach, as a function of the pyrrole dihedral angles $\phi_1, \phi_2, \phi_3, \phi_4$. These maps have been constructed considering the data of **P-H₄TPPS₄²⁻**, with all the four dihedral sulfonato-phenyl angles positive.

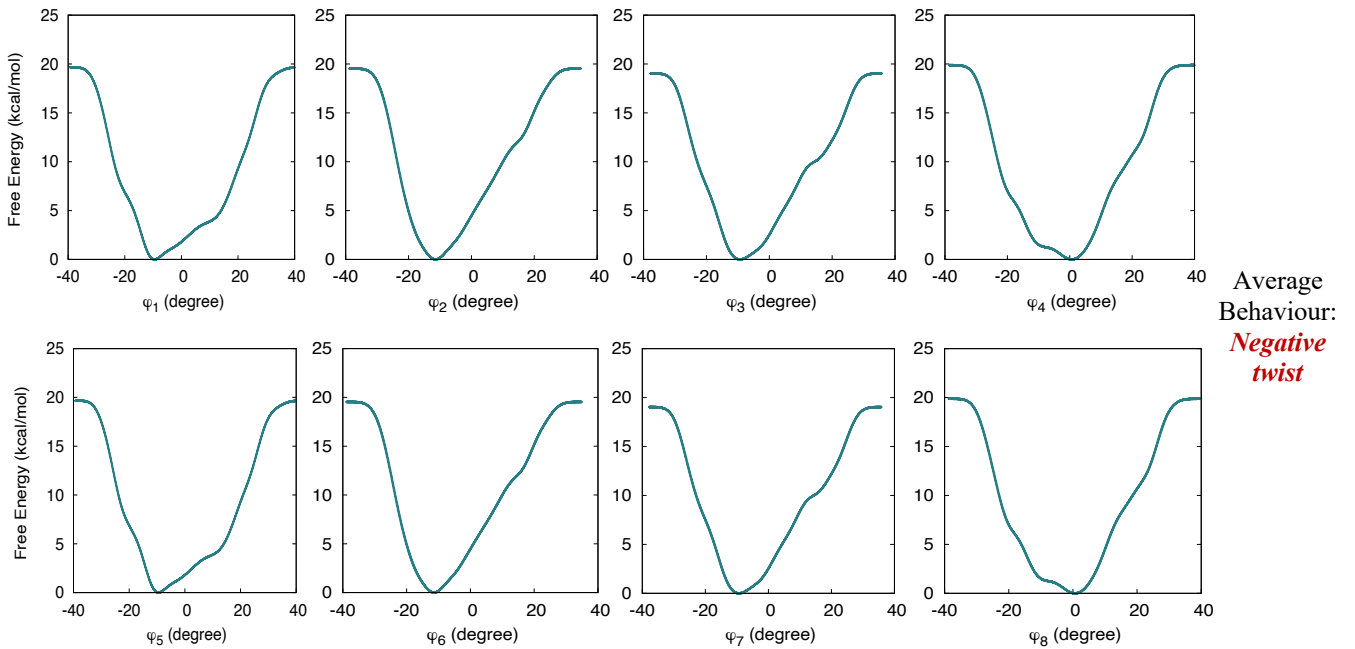


Figure S17. Monodimensional free-energy profiles computed for the **M-H₄TPPS₄²⁻** dimer within the PB-MetaD approach, as a function of the pyrrole dihedral angles $\phi_1, \phi_2, \phi_3, \phi_4$. These maps have been constructed considering the data of **M-H₄TPPS₄²⁻**, with all the four dihedral sulfonato-phenyl angles negative.

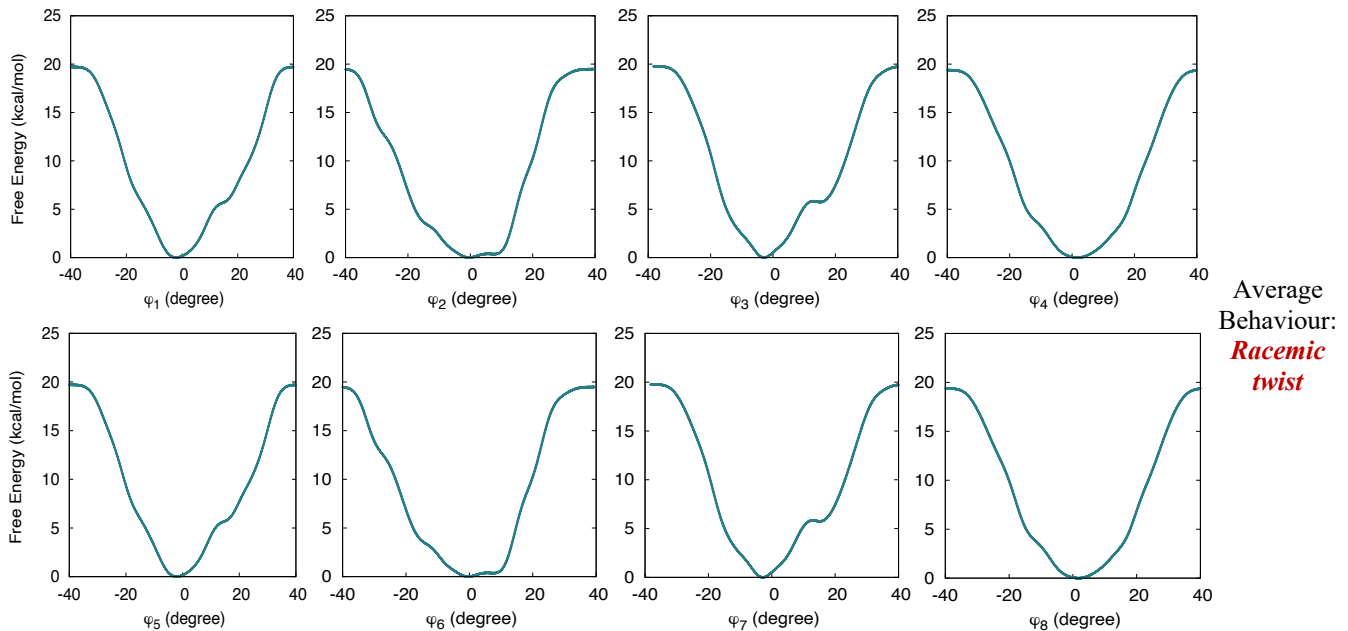


Figure S18. Monodimensional free-energy profiles computed for the **Rac-H₄TPPS₄²⁻** dimer within the PB-MetaD approach, as a function of the pyrrole dihedral angles $\phi_1, \phi_2, \phi_3, \phi_4$. These maps have been constructed considering the data of **Rac-H₄TPPS₄²⁻**, with two dihedral sulfonato-phenyl angles positive and two negative.

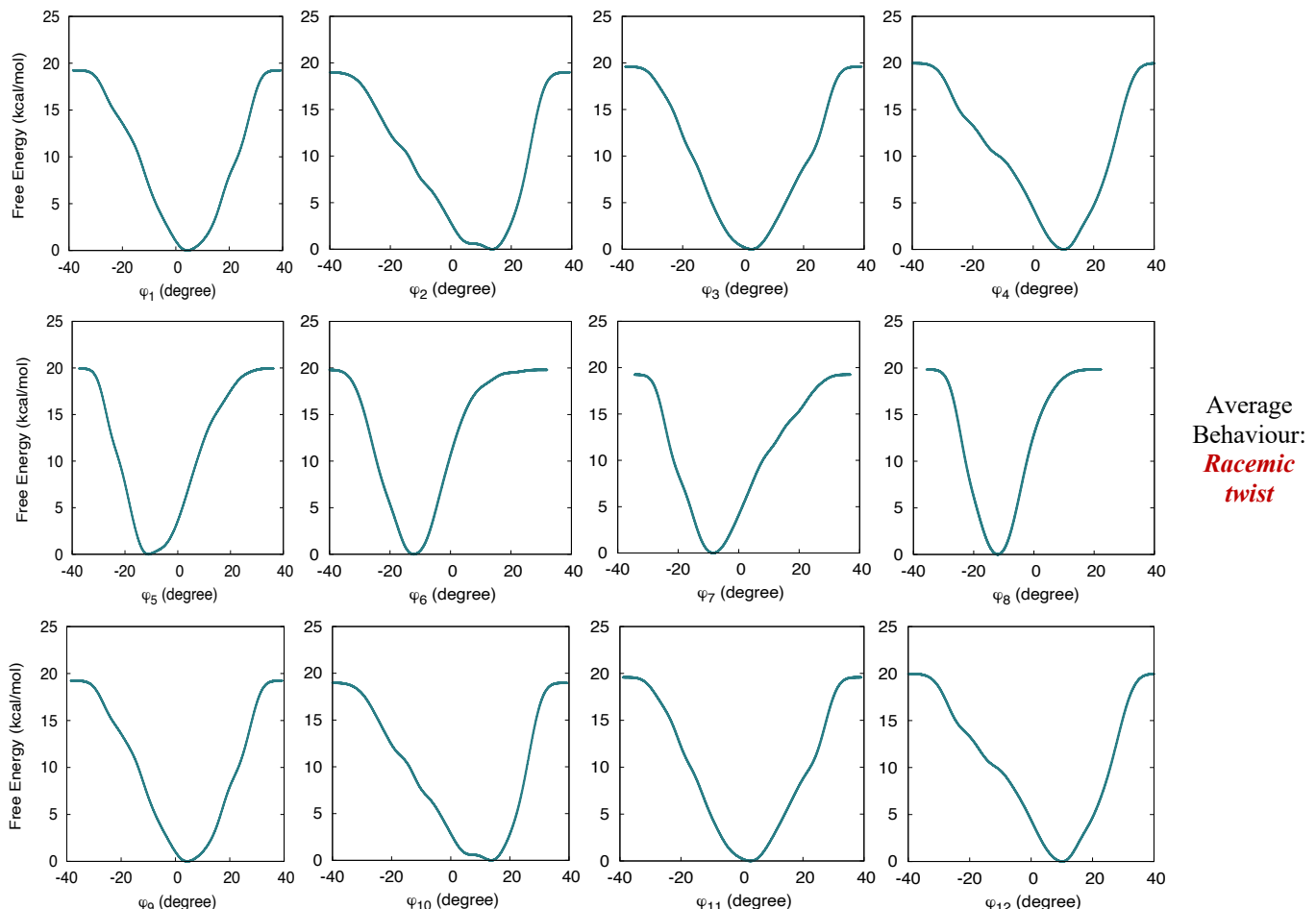


Figure S19. Mono-dimensional free-energy profiles computed for the **P-H₄TPPS₄²⁻** trimer using the MW-MetaD approach, as a function of the pyrrole dihedral angles $\phi_1, \phi_2, \phi_3, \phi_4, \phi_5, \phi_6, \phi_7, \phi_8$. These maps have been constructed considering the data of **M-H₄TPPS₄²⁻**, having all the four sulfonato-phenyl dihedrals positive. a) Free energy profiles of external and b) internal porphyrin rings.

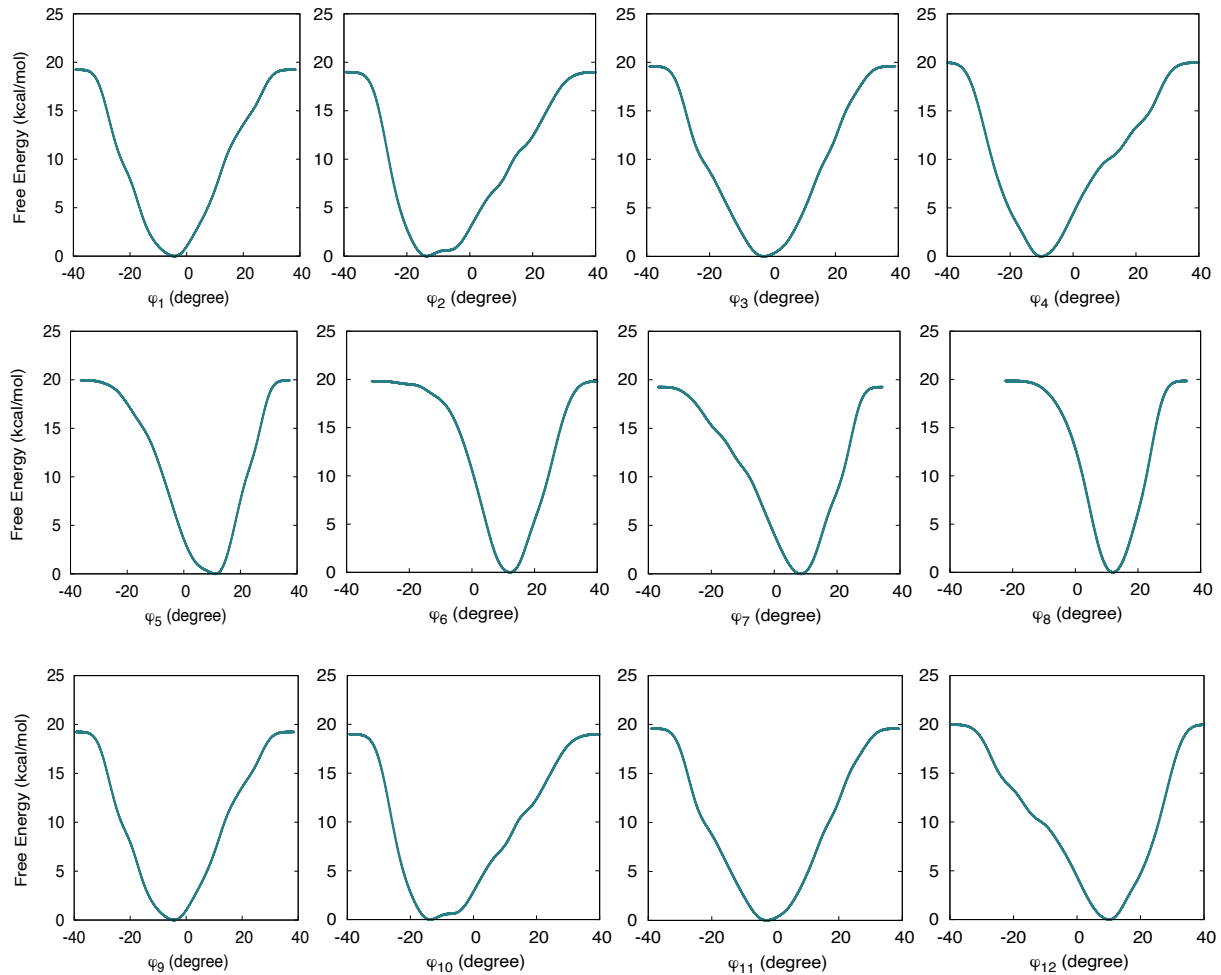


Figure S20. Mono-dimensional free-energy profiles computed for the $\text{M-H}_4\text{TPPS}_{4^2^-}$ -trimer using the PB-MetaD approach, as a function of the pyrrole dihedral angles $\phi_1, \phi_2, \phi_3, \phi_4, \phi_5, \phi_6, \phi_7, \phi_8$. These maps have been constructed considering data of $\text{M-H}_2\text{TPPS}_{4^2^-}$, having all the four sulfonato-phenyl dihedrals negative. a) Free energy profiles of external and b) internal porphyrin rings.

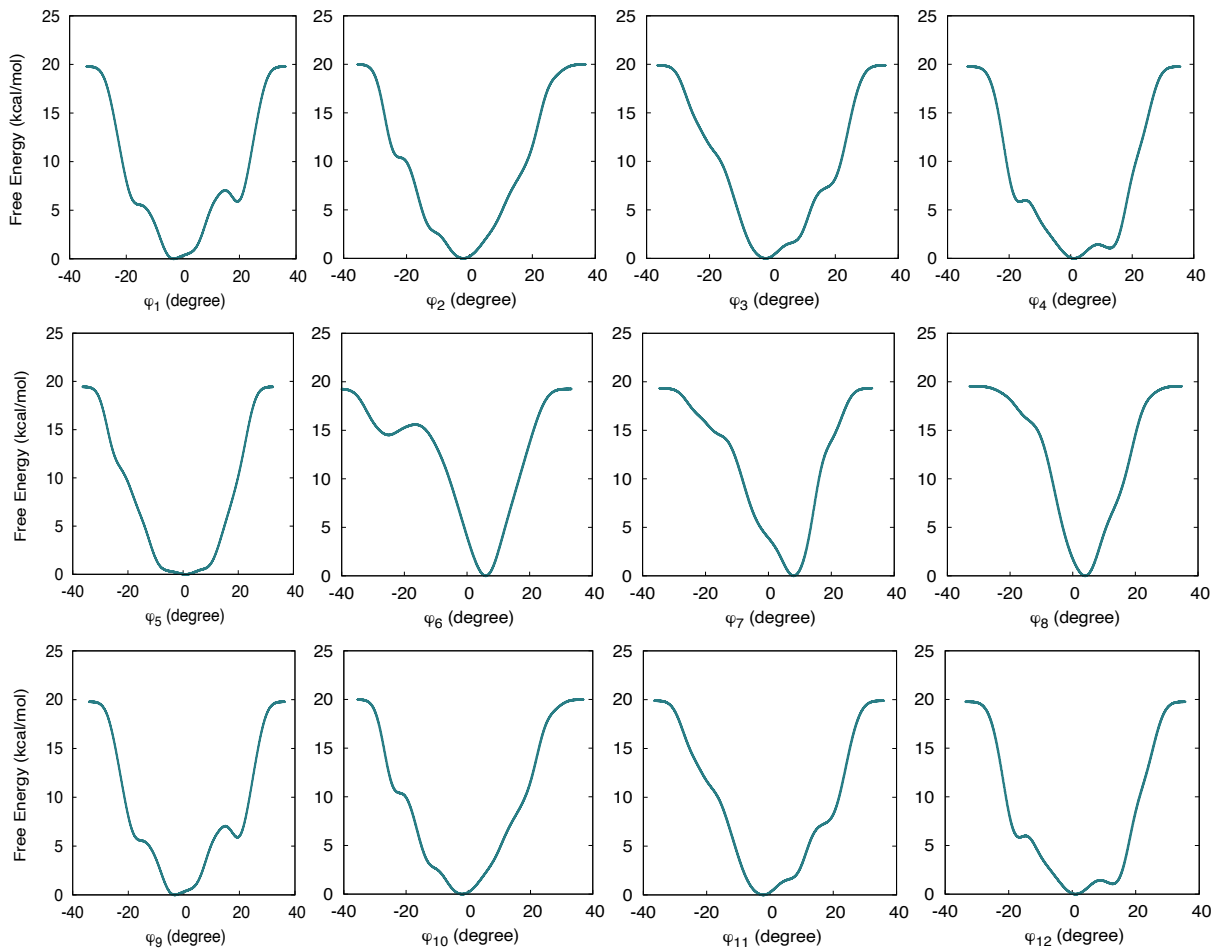
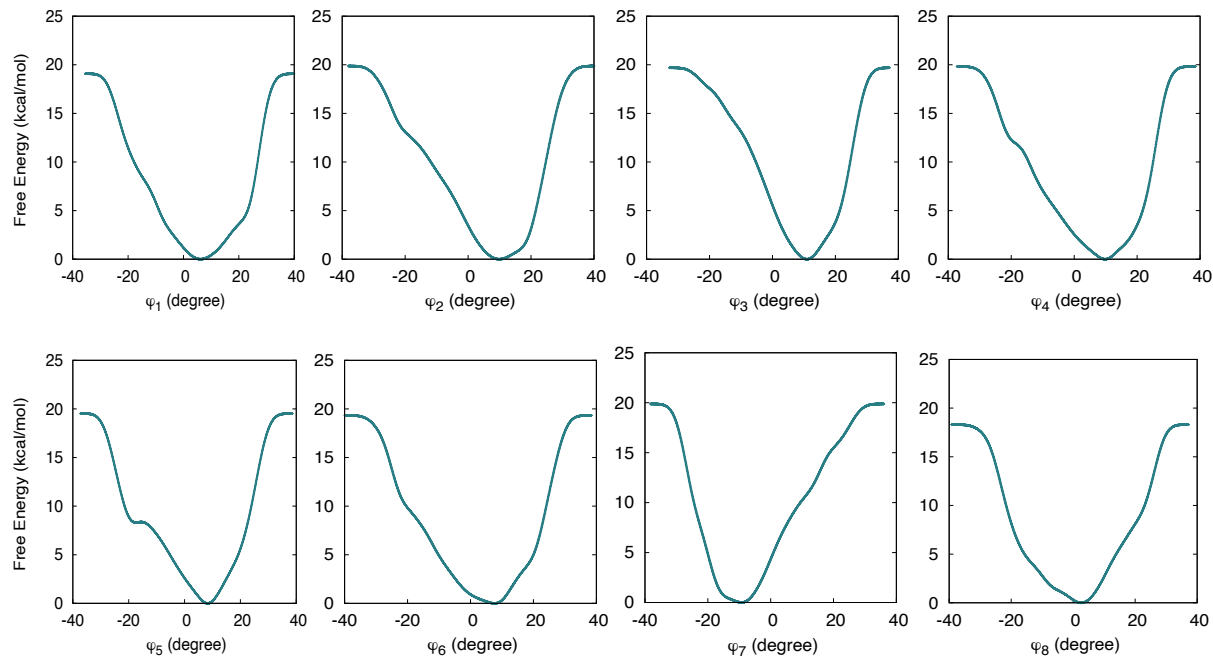


Figure S21. Mono-dimensional free-energy profiles computed for the **Rac-H₄TPPS₄²⁻** trimer using the PB-MetaD approach, as a function of the pyrrole dihedral angles $\phi_1, \phi_2, \phi_3, \phi_4$. These maps have been constructed considering data of **Rac-H₄TPPS₄²⁻**, having the two sulfonato-phenyl dihedrals positive and the other two negative. a) Free energy profiles of external and b) internal porphyrin rings.



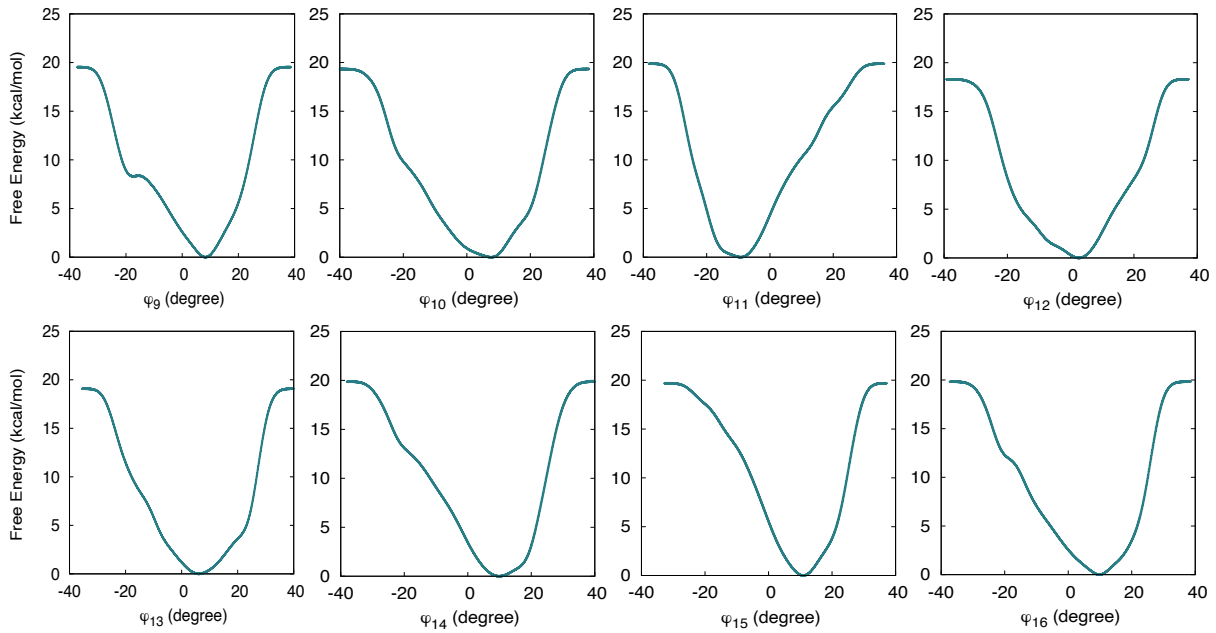
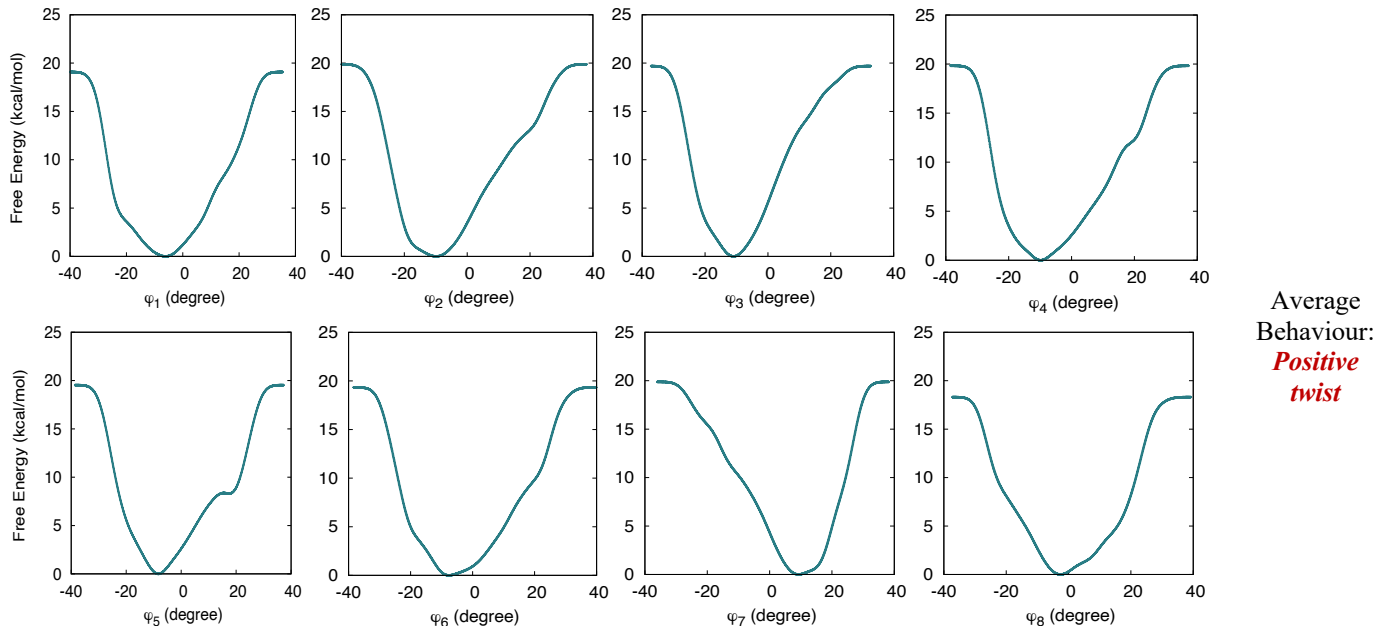


Figure S22. Mono-dimensional free-energy profiles computed for the $\text{P-H}_4\text{TPPS}_4^{2-}$ tetramer using the MW-MetaD approach, as a function of the pyrrole dihedral angles $\phi_1, \phi_2, \phi_3, \phi_4, \phi_5, \phi_6, \phi_7, \phi_8$. These maps have been constructed considering data of $\text{P-H}_4\text{TPPS}_4^{2-}$, having the four dihedral sulfonato-phenyl angles positive. a) Free energy profiles of a) external and b) internal porphyrin rings.



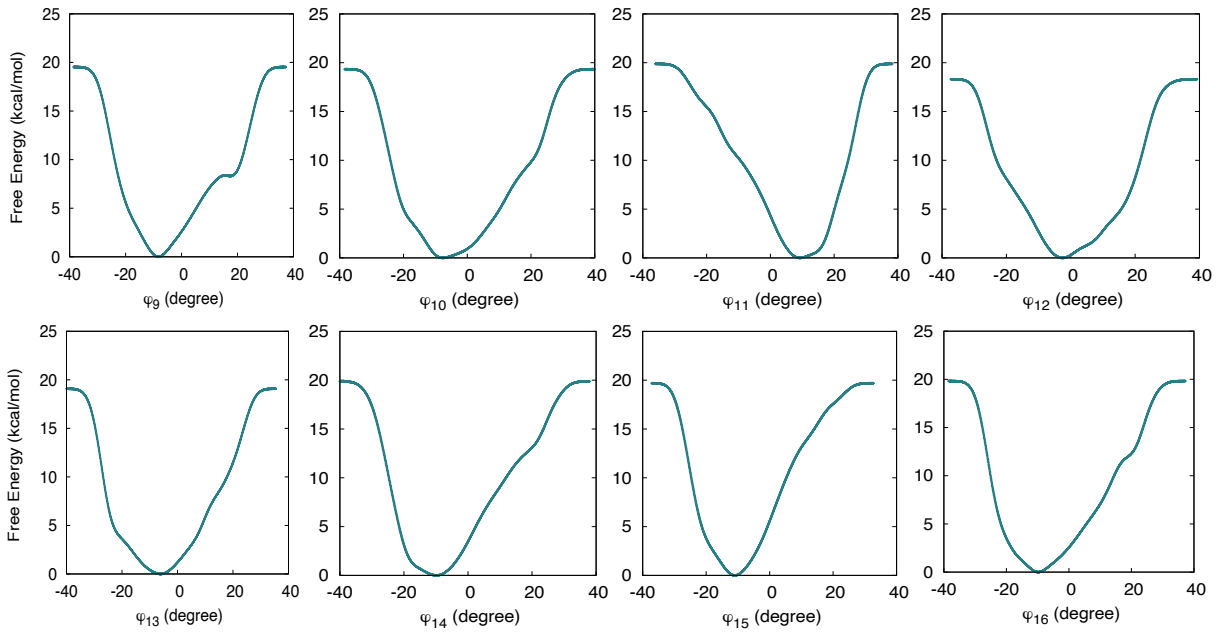
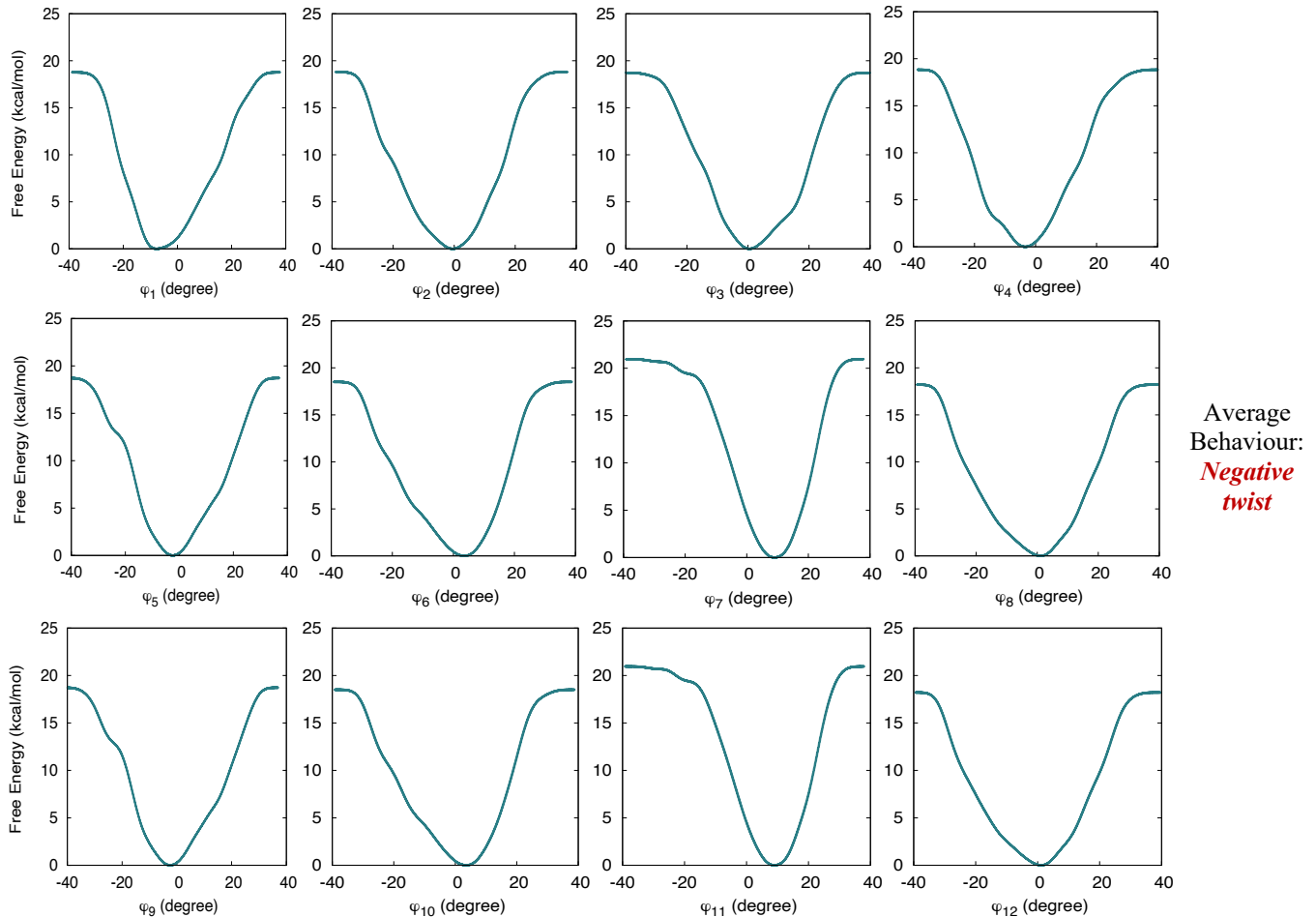


Figure S23. Mono-dimensional free-energy profiles computed for the $\text{M-H}_4\text{TPPS}_4^{2-}$ tetramer using the MW-MetaD approach, as a function of the pyrrole dihedral angles $\phi_1, \phi_2, \phi_3, \phi_4, \phi_5, \phi_6, \phi_7, \phi_8$. These maps have been constructed considering data of $\text{P-H}_4\text{TPPS}_4^{2-}$, that is structure that have all four dihedral sulfonato-phenyl angles negative. a) Free energy profiles of external porphyrin rings and b) free energy profiles of internal porphyrin rings.



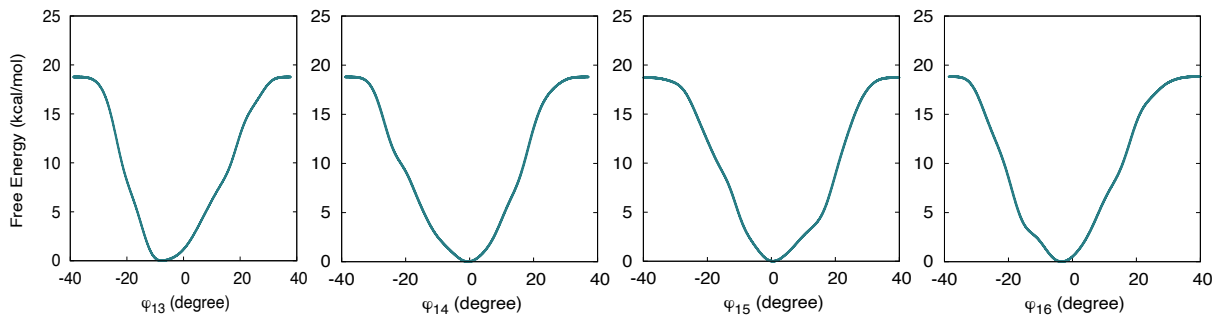


Figure S24. Mono-dimensional free-energy profiles computed for the **Rac-H₄TPPS₄²⁻** tetramer using the MW-MetaD approach, as a function of the pyrrole dihedral angles ϕ_1 , ϕ_2 , ϕ_3 , ϕ_4 , ϕ_5 , ϕ_6 , ϕ_7 , ϕ_8 . These maps have been constructed considering data of P-H₄TPPS₄²⁻, that is structure that have all four dihedral sulfonato-phenyl angles positive. a) Free energy profiles of external porphyrin rings and b) free energy profiles of internal porphyrin rings.